Thermochimica Acta, 235 (1994) 239–253
Elsevier Science B.V., Amsterdam
SSDI 0040-6031(93)01562-H

A kinetic and mechanistic study of the thermal decomposition of rubidium permanganate

Andrew K. Galwey [a,*], Shirley A. Lyle [a] and Seham A.A. Mansour [b]

[a] *School of Chemistry, The Queen's University of Belfast, Belfast BT9 5AG (UK)*
[b] *Department of Chemistry, Minia University, El Minia (Egypt)*

(Received 15 July 1993; accepted 21 August 1993)

Abstract

We report a study of the thermal decomposition of rubidium permanganate. Isothermal kinetic measurements of the evolved oxygen produced showed a sigmoid fractional reaction α–time relation with a rate maximum at $\alpha \approx 0.65$. Data fit the power law $\alpha^{1/3} = kt$ in the range $0.04 < \alpha < 0.6$–0.7; this is an unusually extended acceleratory phase. Subsequently, decomposition is relatively rapid and is completed in a short deceleratory process. The results are not satisfactorily expressed by rate equations characteristic of solid-state reactions and it is concluded that local and/or temporary melting participates in controlling the kinetic behaviour. Some fusion of the product is consistent with the textural changes that accompany salt decomposition, as revealed by scanning electron microscopy. We conclude that, with the participation of local and perhaps temporary melting, the overall decomposition contains features of both homogeneous and heterogeneous reaction mechanisms.

INTRODUCTION

This kinetic study of the thermal decomposition of rubidium permanganate is a contribution towards a wider re-examination of the mechanisms of thermal reactions of alkali permanganates. The present results are discussed in the context of recently completed studies of the decompositions of $CsMnO_4$ [1] and $KMnO_4$ [2]. Further work on $LiMnO_4$ [3] is in progress. The mechanisms of the thermal breakdown of these compounds, $KMnO_4$ in particular, are not yet completely understood and papers on the topic continue to appear [1, 2, 4]. A classic investigation of the thermal decomposition of potassium permanganate made a notable contribution to the theory of solid-state kinetics [5]. Following recent developments in microscopy, we identified the thermal reactions of permanganates as a topic suitable for future research in the context of advances in the subject [4].

Three main aspects of the thermal breakdown of $RbMnO_4$ were investigated in the present work. The interpretation of isothermal kinetic measure-

* Corresponding author.

ments was considered with particular reference to the earlier reported fit to the Prout–Tompkins equation [4–6], previously described as very satisfactorily representing $KMnO_4$ decomposition [5]. More recently, the Avrami–Erofe'ev equations [4] have found wider applications in kinetic analyses of solid-state thermal rate processes. It was of interest, therefore, to compare the fit of data for isothermal $RbMnO_4$ decomposition to these solid-state kinetic expressions. Secondly, we have applied the greater resolving power of the scanning electron microscope, not available during the early work, to the characterization of the textural changes that accompany reaction. Our interpretation of kinetic results can, therefore, include consideration of this complementary evidence which is valuable in formulating the reaction mechanism. Finally, the rate controlling process in anion breakdown is discussed with reference to the role of electron transfer in the anionic sub-lattice, as discussed by Boldyrev [7].

There have been several previous studies of the thermal decomposition of $RbMnO_4$. Herley and Prout [6] concluded that the kinetic characteristics of this reaction resembled the behaviour of $KMnO_4$. The sigmoid-shaped isothermal fractional reaction α–time curve fitted the Prout–Tompkins equation in two ranges with different rate constants during the acceleratory and the decay processes. Pre-irradiation accelerated the onset of reaction [8]. The residual reaction products have been analysed [9]. Erenburg et al. [10] conclude that, in contrast to the potassium salt, $Rb_3(MnO_4)_2$ is not formed as a reaction intermediate. Further aspects of the decomposition of $RbMnO_4$ have been reported by Booth et al. [11] and by Gontarz and Pisarska [12]. Literature concerned with the closely similar decompositions of $KMnO_4$ and of $CsMnO_4$ have been cited in refs. 2 and 1, respectively.

EXPERIMENTAL

Apparatus

Kinetic studies of $RbMnO_4$ decomposition were carried out in a pre-evacuated ($<10^{-4}$ Torr) conventional glass apparatus. The extent of reaction was calculated from oxygen pressures evolved in the known volume of the vacuum envelope using an MKS 222B absolute pressure diaphragm gauge (0–10 Torr, read ± 0.001 Torr). Time, pressure and temperature readings were recorded automatically at specified time intervals and the data stored in the computer memory for later analysis. Details of the apparatus have been described [13]. Computing facilities enabled results to be presented in tabular or in graphical forms, using calculated values of fractional reaction α or the appropriate kinetic functions $f(\alpha)$ [4] at recorded times.

Weighed reactant samples, usually 30–40 mg (± 0.2 mg) $RbMnO_4$, were evacuated 1 h prior to decomposition. In some experiments, a cold trap (78 K) was maintained between the reactant, heated at constant tempera-

ture (± 0.7 K), and the gauge, in order to condense products other than oxygen, including any water retained as an impurity in the crystals of $RbMnO_4$.

Reactant solid: $RbMnO_4$

The sparingly soluble reactant was prepared by precipitation on mixing cold aqueous solutions containing stoichiometrically equivalent amounts of Rb_2SO_4 and $KMnO_4$. The precipitate was retained with the solution for 24 h to permit crystal growth. The prepared salt, separated by filtration, was washed with cold water, dried in air and stored in a dark bottle. Storage periods were short; reactions were completed soon after salt preparation. Two separate, but similarly prepared, samples of $RbMnO_4$ were used during the present kinetic and microscopic studies.

Electron microscopy

The textural changes that occurred during reactions were observed using a Jeol 35CF scanning electron microscope. Specimens of reactant, of product and of salt, partially decomposed to appropriate α values, were examined. Some specimens were lightly crushed after decomposition to fracture crystals, thereby exposing sections that revealed the topographical changes that had occurred during chemical changes inside the reactant particles. All specimens examined were precoated with a thin Au/Pd film to render surfaces conducting. Only features that were reproducible and typical of the significant textural changes that occurred during reaction were photographed.

RESULTS AND DISCUSSION

Reaction stoichiometry

The total yield of the uncondensed gaseous product, oxygen, was directly proportional to the reactant weight and, within the range studied (480–560 K), was independent of reaction temperature. The mean stoichiometry of the decomposition, determined both from weight loss and from the pressure of gas evolved in the known apparatus volume, was 0.57 ± 0.02 mol O_2 per mol $RbMnO_4$ decomposed. Permanganate ion breakdown was $\geqslant 96\%$ complete, as measured by oxalate titration of the residual products. All maxima present in the X-ray diffraction patterns recorded for the residue corresponded qualitatively and quantitatively with expectation [10] for Rb_2MnO_4. There was also diffuse X-ray scattering indicating that a proportion of the residue was poorly crystallized or amorphous.

The present observations are, therefore, in very satisfactory agreement with previously published [6, 8, 9] stoichiometric conclusions for this reaction (the bracketed constituent has not yet been fully characterized)

$$RbMnO_4 \rightarrow 0.57O_2 + xRb_2MnO_4 + [Rb_{1-2x}Mn_{1-x}O_{2.86-4x}]$$

Electron microscopy

We find it convenient to report our microscopic observations before the kinetic results so that interpretation of the rate data can include consideration of the topographical modifications that occur as decomposition proceeds. We are aware of no previous use of scanning electron microscopy to characterize the textural changes during $RbMnO_4$ breakdown. Herley and Prout [6, 8], using optical microscopy, report the occurrence of longitudinal splitting of reactant crystals during decomposition. There was some diminution in the average particle size during the accelerating phase of the reaction.

Unreacted $RbMnO_4$ crystallites were bounded by (approximately) flat and usually smooth faces which, however, were often pitted and had rounded corners. Crystal shapes and sizes in the present preparations were variable, see Fig. 1; some were approximately equidimensional while others were elongated in one dimension (up to approx. 0.5 mm).

There was strong evidence that decomposition was accompanied by textural modification of the reactant beneath a thin (approx. 0.05 μm) superficial boundary layer that itself underwent very little modification or change in appearance during decomposition, see Fig. 2 (where $\alpha = 0.20$ after reaction at 530 K). Similar behaviour has already been described for $KMnO_4$ [2] and $CsMnO_4$ [1]. Microscopic observations were, therefore, focussed on zones where the boundary layer had become detached (as seen in the central area of Fig. 2 and shown at higher magnification in Fig. 3) and at crystal interiors revealed in section by fracture on cold working after reaction. Figure 3 shows textures recognized as typical of the decomposed salt. These are parallel cracking, together with rounded surfaces of constituent crystals. Figure 4 shows similar features on a different crystal from the same reacted sample.

Parallel reactant cracking, together with rounded surfaces of boundary crystallites, is also evident in salt decomposed to $\alpha = 0.55$ at 530 K; representative textures are shown in Figs. 5 and 6. While the residue from the completed decomposition ($\alpha = 1.00$ at 490 K) gave evidence of some particle disintegration, it appeared that most crystallites remained coherent and retained the smooth outer boundary surfaces. Removal of this outer layer (again) revealed subsurface reactant cracking and the intraparticulate material was largely composed of rounded particles, see Figs. 7 and 8.

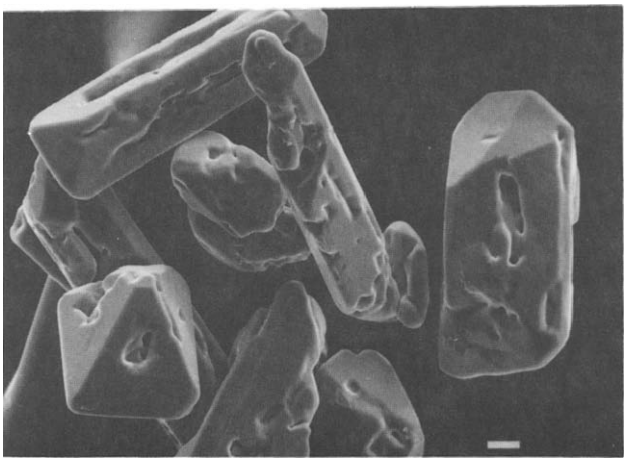

Fig. 1. Typical crystals of the $RbMnO_4$ reactant. Some crystals are approximately equidimensional and others are elongated in one dimension. Surfaces are smooth and corners rounded, but many crystal faces are extensively pitted. Scale bar, 10.0 μm.

Comment

The reactant underwent no comprehensive melting during reaction. The superficial material, evidently unreactive, appeared to have inhibited the possibility of intercrystalline interaction or sintering. This layer, perhaps evidence of enhanced reactivity of the crystal boundary, may have developed during storage or more probably during, or immediately following, heating to reaction temperature. The extent of this process is, however, limited and represents only a small proportion of the decomposition (approx. 2–4%).

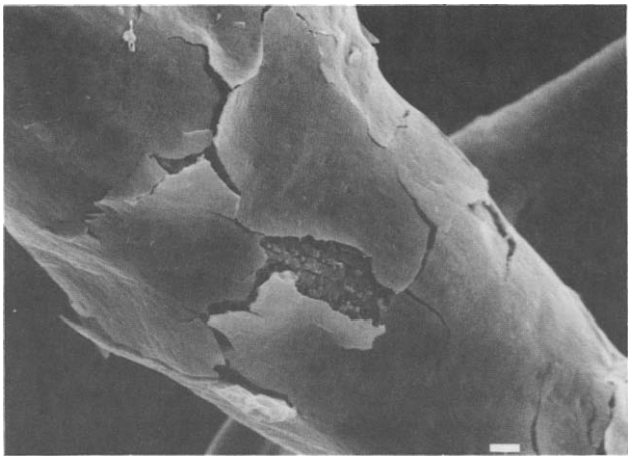

Fig. 2. Surfaces of the decomposed salt ($\alpha = 0.20$, 530 K) are bounded by a thin (approx. 0.05 μm) adherent superficial layer, the outer face of which is smooth, resembling that of unreacted salt. The textural changes resulting from reaction are revealed where mechanical damage has removed a segment of the covering (see Fig. 3). Scale bar, 1.0 μm.

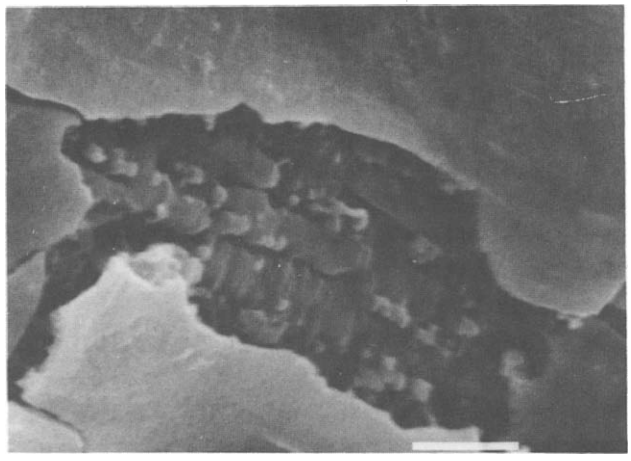

Fig. 3. Larger magnification view of the area from Fig. 2 where the covering layer is removed. The texture exposed is characteristic of the reacted salt: approximately parallel, but often irregular, cracking and rounded surfaces of the intracrystalline adherent assemblage. Scale bar, 1.0 μm.

The main decomposition was accompanied by some intracrystalline cracking, consistent with the Prout–Tompkins model [5, 6] and expected because of reactant contraction consequent upon loss of constituent oxygen. The results do not, however, give unambiguous or comprehensive support to the operation of a crack disintegration model [5]. There are positive indications that during reaction there was intraparticulate sintering to

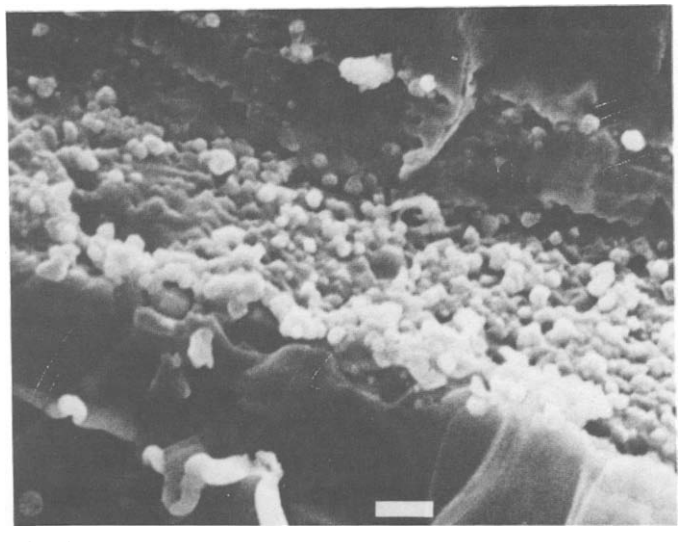

Fig. 4. Reacted zone of a different crystal from the same reacted sample as that in Figs. 2 and 3. The rounded texture of the product particles suggests melting or sintering. Scale bar, 1.0 μm.

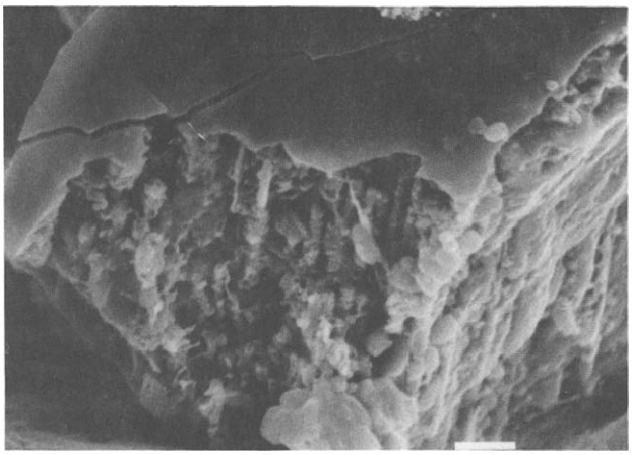

Fig. 5. Reacted zone of crystal partially decomposed to $\alpha = 0.55$ at 530 K: features exposed on removal of superficial outer layer. Salt decomposition is characterized by parallel cracking and the development of rounded particles. Scale bar, 1.0 μm.

maintain the coherent aggregates that were the original reactant crystals. The rounded boundaries of the crystallites within the reacted material suggest textural control by surface free-energy considerations. There was no evidence of the aligned crack development within decomposed material that would be expected from the strain-fracture model proposed to explain Prout–Tompkins behaviour [4–6]. Moreover, there was no development of regular prisms with flat and oriented faces that would result from growth of a crystalline product during decomposition [2]. There must be at least

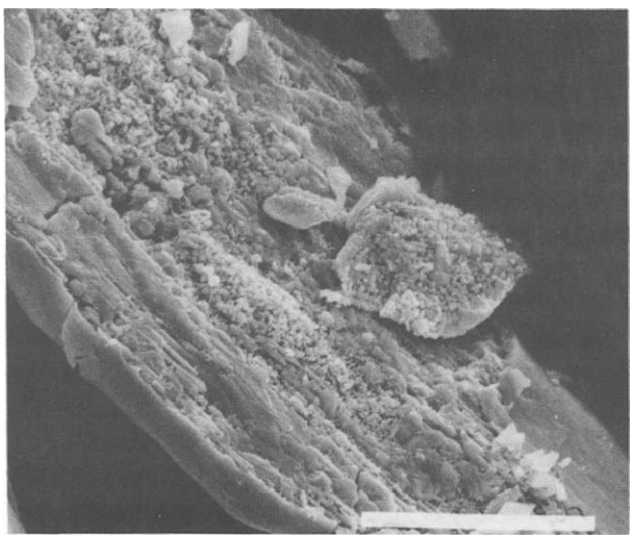

Fig. 6. Another crystal from the same batch as in Fig. 5 showing features similar to those in Figs. 4 and 5. Scale bar, 10.0 μm.

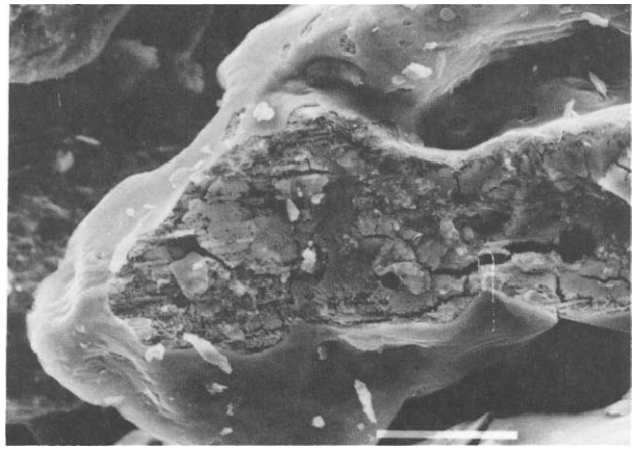

Fig. 7. Smooth outer surfaces and intraparticular crack structure revealed on removal of outer layer in decomposed crystal, $\alpha = 1.00$ at 490 K. The crack disposition is irregular with no evident alignment and the product aggregate remains pseudomorphic with the original reactant crystals. Scale bar, 10.0 μm.

superficial mobility of reactant and/or product material within the reaction zone, perhaps with segregation of components including the crystalline Rb_2MnO_4. This is envisaged as including local and/or temporary melting, from which some poorly crystallized or amorphous material remains in the residual product. We sought, but found no evidence of, those features expected to be present if reaction proceeded by an advancing interface model [4]. It seems most probable that there was (at least) some, perhaps restricted, mobility of the species participating in anion breakdown. It is not possible, however, to establish from these microscopic observations whether or not the reaction zone was molten during reaction.

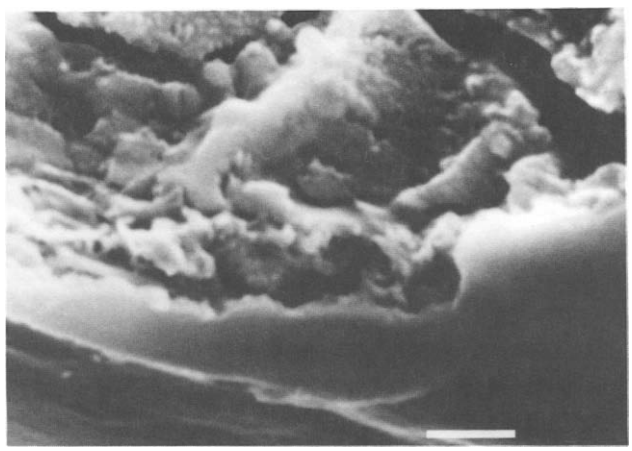

Fig. 8. Another crystal from the batch as in Fig. 7. Particles of product are rounded and sintered, indicative of possible local and temporary melting. Scale bar, 1.0 μm.

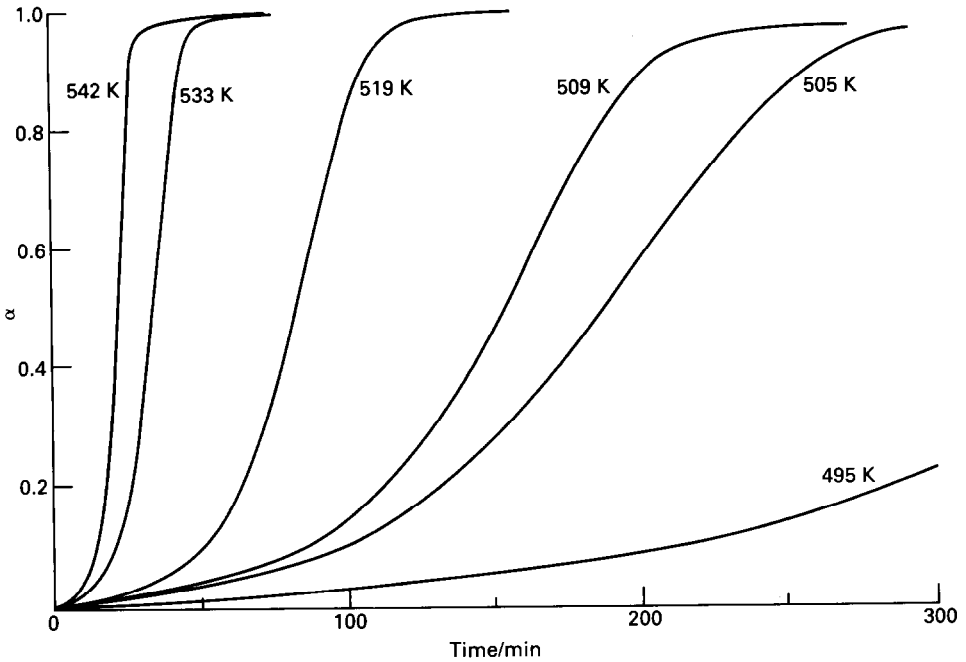

Fig. 9. Typical α–time plots for the isothermal decomposition of $RbMnO_4$ at six representative temperatures between 495 and 542 K. Curves are sigmoid shaped with a prolonged acceleratory phase to $\alpha \approx 0.65$.

Reaction kinetics

Kinetic measurements were based on oxygen evolution during the decompositions of our two prepared samples of $RbMnO_4$, between 480 and 550 K. The typical sigmoid α–time plots in Fig. 9 were predominantly acceleratory. The point of inflection, measured from maxima on $d\alpha/dt$ against α plots, Fig. 10, were at $\alpha =$ approx. 0.65 ± 0.05 which agrees with previous work [6, 8], although in these articles specific values of this parameter were not reported.

From an extensive kinetic analysis of our data we conclude that the power law

$$\alpha^{1/3} = kt$$

provided the most satisfactory quantitative description of the reaction rates in the range $0.04 < \alpha < 0.6$–0.7. The fit of data from Fig. 9 to this equation is shown in Fig. 11. These linear plots extrapolate close to $\alpha = 0$ and $t = 0$, which we regard as further support for the applicability of this kinetic relation. Plots of $\ln \alpha$ against time, the exponential equation [13], were also close to linearity in the range $0.04 < \alpha < 0.6$, Fig. 12. This was unexpected because the differential plots (the more sensitive test) were not linear, Fig.

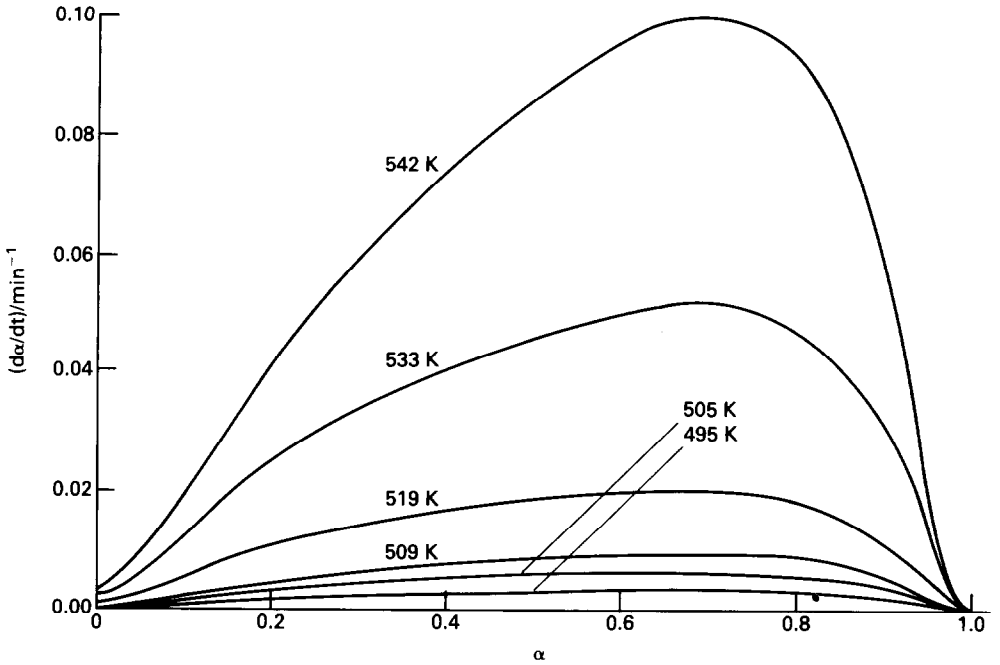

Fig. 10. Differential plot, $d\alpha/dt$ against α, for the data of Fig. 9.

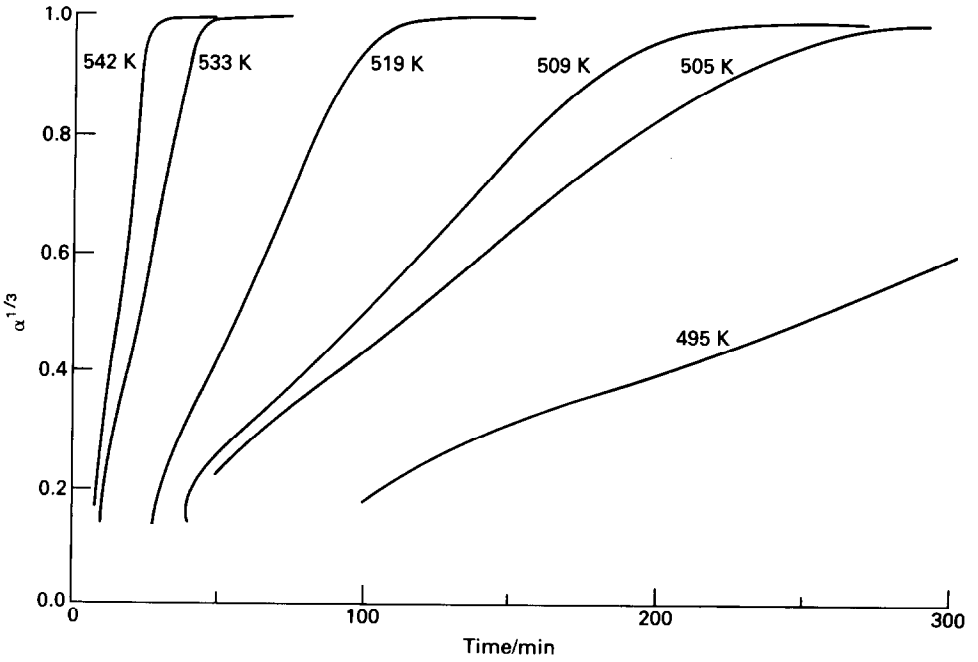

Fig. 11. Power law plots, $\alpha^{1/3}$ against time, for the data in Fig. 9. Satisfactory linearity is observed in the range $0.04 < \alpha < 0.6$.

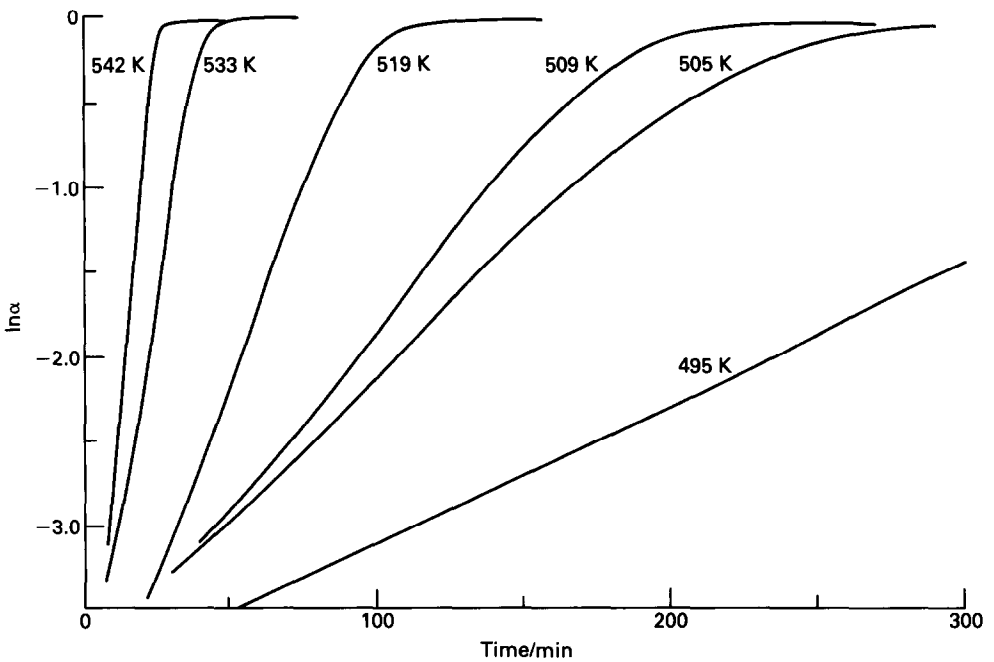

Fig. 12. Exponential law plots, $\ln \alpha$ against time, for data in Fig. 9. Again the plot is approximately linear, see discussion in text.

10. (This comparison is made because integration of $d\alpha/dt = kt$ gives $\ln \alpha = kt$.) This apparent inconsistency is a consequence of the insensitivity for kinetic testing of integrated functions that give logarithmic plots.

During our extensive tests of kinetic expressions applicable to solid-state reactions [4], none was found that fitted the data across the whole reaction including both the acceleratory and deceleratory phases. Plots for the Avrami–Erofe'ev equations, $n = 2$, 3 or 4, and the Prout–Tompkins equation [4] were curved, apparently exhibiting *relatively* acceleratory behaviour during the later stages. While plots of these functions exhibited two linear regions, the second rate constant was always the greater [6]. The intermediate portion, joining the two linear regions, was often curved: this was regarded as an unsatisfactory feature of the analysis. Thus, we identify none of the rate equations tested as providing a quantitative and acceptable description of the kinetic characteristics overall.

The mean calculated activation energy for $RbMnO_4$ decomposition for $0.05 < \alpha < 0.65$ and 480–550 K was 165 ± 5 kJ mol^{-1}. Data for both samples were close to a single line on each of two Arrhenius plots using rate constants from the power law ($\alpha^{1/3} = kt$) and the exponential law ($\ln \alpha = kt$) plots. This result agrees with previously reported values, 165–170 kJ mol^{-1} [6, 8].

The onset of reaction

Induction periods to the onset of decompositions were invariably short. Large scale α–time plots showed an initial zero-order process when $\alpha < 0.03$ that extrapolated to the time axis at 0–5 min, the time required for sample heating. This initial reaction may be responsible for the generation of the superficial outer product layer seen in Fig. 2. When $\alpha > 0.03$, the reaction became acceleratory.

Crushed reactant

The kinetic characteristics of the decompositions of samples of salt crushed before reaction were almost indistinguishable from the uncrushed material. The only small influence was a just detectable rise in reaction rate during the acceleratory phase when $\alpha < 0.15$. Decompositions of crushed mixtures containing previously decomposed material ($\alpha = 1.00$) showed a further slight enhancement of the initial reaction rate. These effects were, however, small and at the limits of detection.

Pre-admission of a small water vapour pressure (approx. 5 Torr H_2O) to the reaction vessel, which remained present during reaction, caused no detectable change in the salt decomposition rate.

Decompositions of 1:1 molar $RbMnO_4 + CsMnO_4$ mixtures

These studies were undertaken to determine whether decompositions of $RbMnO_4 + CsMnO_4$ 1:1 molar mixtures proceeded more rapidly than the sum of the reaction rates of constituents. There was the possibility that anion breakdown would be promoted in a mixed melt or in a eutectic formed between the salts.

Similarly crushed samples of reactants prepared containing the individual salts and the mixture were reacted at 535 ± 1 K. Decomposition in the mixture showed two rate maxima at 32 and 75 min, which closely corresponded with the behaviours of the individual pure salt, and rates were $\times 0.5$. Thus, results for the mixture demonstrate positively that the decompositions of each of the two components were independent of the presence of the other.

CONCLUSIONS

The kinetic analysis of $RbMnO_4$ decomposition was incomplete because we identified no rate equation that adequately and completely represented the sigmoid α–time curves. The fits to the Avrami–Erofe'ev equations ($n = 2$, 3 or 4) were less than satisfactory. We also confirm obedience to the Prout–Tompkins equation but note that there were two rate constants of which the second is the greater.

The prolonged acceleratory character of this reaction (maximum rate at $\alpha \approx 0.65$) is unusual. Rate processes in the solid-state do not usually fit the

power law across this extended range ($0.03 < \alpha < 0.6$). The tendency towards a progressive increase in rate during the reaction can also be perceived in the final relatively brief but strongly deceleratory approach to $\alpha = 1.00$. We regard this overall pattern of kinetic behaviour as uncharacteristic of solid-state decompositions. We also note that no realistic rate model can be based on a homogeneous reaction mechanism which would be expected to exhibit deceleratory behaviour. This is consistent with the microscopic observations that demonstrated the absence of comprehensive melting during this decomposition.

To resolve these perceived difficulties in formulating a reaction mechanism for this thermal reaction of $RbMnO_4$, we consider the present observations in the context of our previous results and conclusions for the reactions of $KMnO_4$ [2] and of $CsMnO_4$ [1]. There are close resemblances between these three reactants and their reaction kinetics during anion breakdown. Erenburg et al. [10] have pointed out that all three reactant crystal structures contain chains of MnO_4^- anions parallel with the *b* crystallographic axis. If decomposition requires electron transfer in the anionic array [7], this virtual identity of structure provides one possible explanation of the similarity of activation energy values for the three compounds (160–170 kJ mol^{-1} [2]). These values were evidently independent of changes in the size of cations (K^+, Rb^+, Cs^+) linking the anion chains in the crystal [10]. Magnitudes of the activation energies for $LiMnO_4$ and $NaMnO_4$ decompositions were smaller, approx. 135 kJ mol^{-1}.

The residual decomposition products from the three salts include unidentified components that are poorly crystallized and possibly contain non-stoichiometric phases and/or amorphous material [9]. $K_3[MnO_4]_2$ has been characterized as an intermediate in $KMnO_4$ decomposition but the appearance of no comparable intermediate could be demonstrated in the reactions of $RbMnO_4$ and $CsMnO_4$ [10]. The following relevant features of the reactions of $KMnO_4$ [2] and of $CsMnO_4$ [1] are identified as significant for the discussion of the present observations.

(i) $KMnO_4$ [2]. From complementary kinetic and microscopic studies it was concluded that $KMnO_4$ decomposition is a nucleation-and-growth reaction. Anion breakdown follows an electron transfer step at the boundary of the disorganized environment of the product material.

(ii) $CsMnO_4$ [1]. $CsMnO_4$ decomposition is a predominantly acceleratory reaction that obeyed the power law ($n = 2$) across an unusually extended range ($0.03 < \alpha < 0.85$). It was concluded that decomposition involved the participation of a melt.

The reactivity of $RbMnO_4$ is intermediate in value. Relative reaction rates, compared from maxima of $d\alpha/dt$ against α plots at 520 K, were $KMnO_4$, 0.16 min^{-1}; $RbMnO_4$, 0.020 min^{-1}; and $CsMnO_4$, 0.008 min^{-1}. This sequence follows that of increasing MnO_4^- spacing in the reactant crystals [10]. The pattern of kinetic characteristics also arguably follows the

same sequence. All three decompositions exhibit sigmoid α–time curves. The range of fit to the power law was less for $RbMnO_4$ than that for $CsMnO_4$ (which was identified as melting during reaction [1]). The kinetic characteristics of the $RbMnO_4$ reaction did not conform to the nucleation-and-growth mechanism proposed for $KMnO_4$ [2]. This pattern of behaviour is explained if it is concluded that $RbMnO_4$ decomposition involves limited melt formation but that the extent is less than in $CsMnO_4$.

The participation of melting explains the acceleratory character of $RbMnO_4$ decomposition: the reaction rate rises as the amount of liquid present increases. It is, however, established from the microscopic observations that liquefaction is not extensive and the later deceleratory process results in a rapid approach to completion ($\alpha = 1.00$). Kinetic characteristics are, therefore, intermediate between the behaviour of copper(II) malonate, where melting is extensive [13], and the solid-state decomposition of $KMnO_4$ [2]. The promotional effect of melting in $RbMnO_4$ is less than that in $CsMnO_4$ [1].

Melt formation is believed to occur in the vicinity of the reactant–product contact interface. The autocatalytic behaviour is ascribed to the progressive increase in the amount of product and, therefore, of melt present as the reaction advances. With concurrent separation of the crystalline product, Rb_2MnO_4, the pattern of behaviour can be regarded as intermediate between decomposition accompanied by melting and a solid-state process. This accounts for the similarity in decomposition rates of the prepared and the crushed samples. It is also supported by the small rise in initial rate on crushing reactant with product; significantly the effect is less than with $CsMnO_4$ [1].

It may be concluded that similar rate-limiting steps control the decompositions of $KMnO_4$, $RbMnO_4$ and $CsMnO_4$ because the activation energies are equal [2]. This may be due to the similarities of crystal structures [10] but alternatively may arise through similar chemical steps within a zone of disorganized product material immediately adjoining the reactant crystal. We also note that the identity of the cation does exert a small influence on overall salt reactivity ($CsMnO_4 < RbMnO_4 < KMnO_4$) but, in this group, does not modify the temperature coefficient of reaction rate. We conclude that decomposition is predominantly controlled by interanionic reactions to yield amorphous/molten material from which Rb_2MnO_4 separates, and a poorly crystallized or amorphous residue of "rubidium manganates" remains.

The microscopic appearance of the residue gives support for the view that decomposition is accompanied by limited and local melting. We find little direct support for progressive crack disintegration of the reactant particles as required in the Prout–Tompkins model [5, 6]. Such features would, however, be obscured by melting/sintering apparent in the product. The decomposition of $RbMnO_4$ is therefore regarded as exhibiting kinetic fea-

tures of both heterogeneous and homogeneous reactions, in which the reaction interface is effectively extended and the decomposition rate increased by local melt formation.

ACKNOWLEDGEMENTS

We thank the staff of the Electron Microscope Unit of The Queen's University of Belfast for their help and advice in obtaining the electron micrographs. S.A.A. Mansour thanks the Egyptian Government for financial support.

REFERENCES

1 A.K. Galwey and S.A.A. Mansour, Thermochim. Acta, 228 (1993) 379.
2 M.E. Brown, A.K. Galwey, M.A. Mohamed and H. Tanaka, Thermochim. Acta, 235 (1994) 255.
3 S.A.A. Mansour, to be published.
4 M.E. Brown, D. Dollimore and A.K. Galwey, Comprehensive Chemical Kinetics, Vol. 22, Elsevier, Amsterdam, 1980.
5 E.G. Prout and F.C. Tompkins, Trans. Faraday Soc., 40 (1944) 488.
6 P.J. Herley and E.G. Prout, J. Phys. Chem., 64 (1960) 675.
7 V.V. Boldyrev, J. Phys. Chem. Solids, 30 (1969) 1215.
8 P.J. Herley and E.G. Prout, J. Inorg. Nucl. Chem., 16 (1960) 16.
9 F.H. Herbstein, G. Ron and A. Weissman, J. Chem. Soc. A, (1971) 1821; (1973) 1701.
10 B.G. Erenburg, L.N. Senchenko, V.V. Boldyrev and A.V. Malysh, Russ. J. Inorg. Chem., 17 (1972) 1121.
11 J.S. Booth, D. Dollimore and G.R. Heal, Thermochim. Acta, 39 (1980) 281, 293.
12 Z. Gontarz and B. Pisarska, J. Therm. Anal., 36 (1990) 2113.
13 N.J. Carr and A.K. Galwey, Proc. R. Soc. London Ser. A, 404 (1986) 101.